CPG-Based Manipulation with Multi-Module Origami Robot Surface

Yuhao Jiang[1], Serge El Asmar[1], Ziqiao Wang[1], Serhat Demirtas[1], and Jamie Paik[1]

***Abstract*—Robotic manipulators often face challenges in handling objects of different sizes and materials, limiting their effectiveness in practical applications. This issue is particularly pronounced when manipulating meter-scale objects or those with varying stiffness, as traditional gripping techniques and strategies frequently prove inadequate. In this letter, we introduce a novel surface-based multi-module robotic manipulation framework that utilizes a Central Pattern Generator (CPG)-based motion generator, combined with a simulation-based optimization method to determine the optimal manipulation parameters for a multi-module origami robotic surface (Ori-Pixel). This approach allows for the manipulation of objects ranging from centimeters to meters in size, with varying stiffness and shape. The optimized CPG parameters are tested through both dynamic simulations and a series of prototype experiments involving a wide range of objects differing in size, weight, shape, and material, demonstrating robust manipulation capabilities.**

***Index Terms*—Soft Robot Applications; Modeling, Control, and Learning for Soft Robots; Multi-Robot Systems; Origami Robot; Surface Manipulation; Central Pattern Generator.**

I. INTRODUCTION

ROBOTIC manipulation has made significant strides in recent years, leveraging advanced control and planning algorithms to demonstrate a variety of automated and precise tasks. Traditional robotic manipulators, typically employing robotic arms and grippers, have shown remarkable versatility in handling objects of different materials and shapes [1]–[3]. When combined with advanced learning-based control strategies [4], these systems can perform intricate tasks such as in-hand manipulations [5]–[7], teleoperation [8], [9], dynamic stabilization [10], dynamic throwing [11], and dressing [12].

Traditional robotic grippers excel in their designed applications but often face scalability challenges when handling objects of varying types and sizes [13]. For instance, "Gripping by Actuation" approaches effectively handle convex objects but show limitations with deformable materials [14]. While controlled-stiffness grippers [15], [16] and grippers with integrated adhesion [17], [18] offer unique advantages for specific object types, achieving versatile manipulation remains an open challenge, particularly for objects at meter-scale and with diverse material properties.

Manuscript received: October 28, 2024; Revised January 21, 2025; Accepted March 9, 2025. This paper was recommended for publication by Editor Yong-Lae Park upon evaluation of the Associate Editor and Reviewers' comments. This work is supported by the European Union's Horizon Europe Research and Innovation Programme under grant No. 101069536.

[1]Reconfigurable Robotics Laboratory, School of Engineering, EPFL, Lausanne, 1005, Switzerland. {yuhao.jiang, serge.elasmar, ziqiao.wang, serhat.demirtas, jamie.paik}@epfl.ch *(Corresponding author: Jamie Paik).*

Code available at: https://doi.org/10.5281/zenodo.15011196.

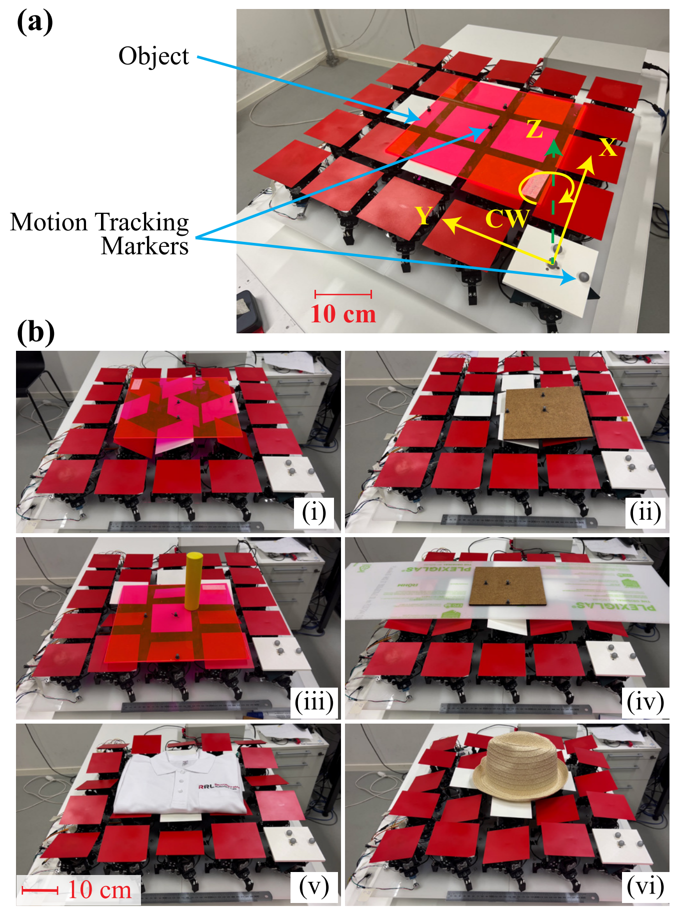

Fig. 1: **Conceptual overview.** (a) Robot setup; (b) experiments demonstrating the system's versatility for manipulating various objects: (i) 300×300 mm acrylic plate, (ii) 200×200 mm wood plate, (iii) 300×300 mm acrylic plate with a slender foam cylinder loosely positioned on top, (iv) 1000×300 mm acrylic plate weighing 1 kg, (v) 400×400 mm Polo shirt weighing 280 g, and (vi) 250×270 mm Trilby hat weighing 55 g.

To address these challenges, researchers have explored alternative approaches such as dynamic planar robotic surfaces. These surfaces, often using arrays of 1-DoF pins or more complex mechanisms like delta robots, have shown promise in manipulating various objects [19]–[24]. However, such systems usually require a significant number of actuators and sophisticated control methods, which limit their applications. Other novel actuators, including soft pneumatic actuators [25], [26], ciliary actuators [27], and liquid crystal elastomers [28], have also been investigated to address these limitations. Nevertheless, these approaches have yet to fully overcome the challenges posed by larger objects or flexible materials.

Central Pattern Generators (CPGs) are widely used for generating rhythmic signals in robotic locomotion, simplifying control and reducing actuation complexity in systems like bipedal [29], [30], quadrupedal [31]–[33], and swimming robots [34], [35]. However, their use in robotic manipulation remains limited.

In this letter, we introduce a novel framework for manipulating objects of diverse sizes and stiffness, ranging from centimeters to meters, using the previously developed multi-module origami robotic surface - Ori-Pixel [36] with the surface-based manipulation concept [37]. This approach combines a collective CPG-based manipulation motion generator with simulation-based optimizations. As shown in Fig. 1(a), our method utilizes the Canfield parallel origami robot, which offers three degrees of freedom: Z-axis translation and rotation around the X and Y axes. By arranging these robots in a 5×5 multi-module array, we enable versatile manipulations including fast and smooth translations and rotations for objects of varying scales and stiffness.

The key challenge in controlling this platform lies in its high dimensionality, with 75 degrees of freedom (DoF) across the array. While this high-DoF configuration provides exceptional flexibility and precision for complex, localized manipulation tasks, it also presents significant challenges for control synthesis. Traditional control methods struggle with the complex kinematics and actuation coordination, while learning-based approaches face difficulties due to the vast search space, challenges in collecting comprehensive training data, and limited adaptability to hardware modifications. For instance, adding or removing a row of modules would typically necessitate complete model retraining in learning-based methods. To address these challenges, we introduce a CPG-based method that strategically groups the modules and represents end-effector motions using synchronized sinusoidal functions, effectively reducing the control optimization targets from 75 individual actuator positions to only 8 parameters. This reduction dramatically simplifies the optimization space, improving both the search efficiency for optimal control parameters and the system's real-world applicability. Moreover, our CPG-based approach offers inherent flexibility to platform modifications, as the underlying control principles remain valid regardless of the specific module configuration.

The proposed framework employs simulation-based optimization of the CPG parameters to generate effective motion patterns across the robotic surface. Through dynamic simulations and prototype experiments, we demonstrate the framework's capability to translate and rotate objects of varying sizes and materials, from rigid wood and acrylic to flexible fabrics. Fine-tuning objective functions allows our CPG-based controller to operate in two distinct modes - fast manipulation and smooth, stable manipulation - with the latter being particularly beneficial for delicate items sensitive to sudden positional and orientational changes, making it an adaptable solution for a broad spectrum of manipulation tasks.

The contributions of this letter are summarized as follows:

1) A novel CPG-based motion generator is developed for manipulations using multi-module robot surface, enabling various collective manipulation modes for objects of diverse sizes and stiffness.
2) A simulation-based optimization framework is then proposed to guide selecting optimal CPG parameters across a range of object settings and manipulation modes.
3) Dynamic simulations and prototype experiments are conducted to validate the proposed motion design and optimization framework, demonstrating effective manipulations of objects with varying sizes, shapes, and stiffness.

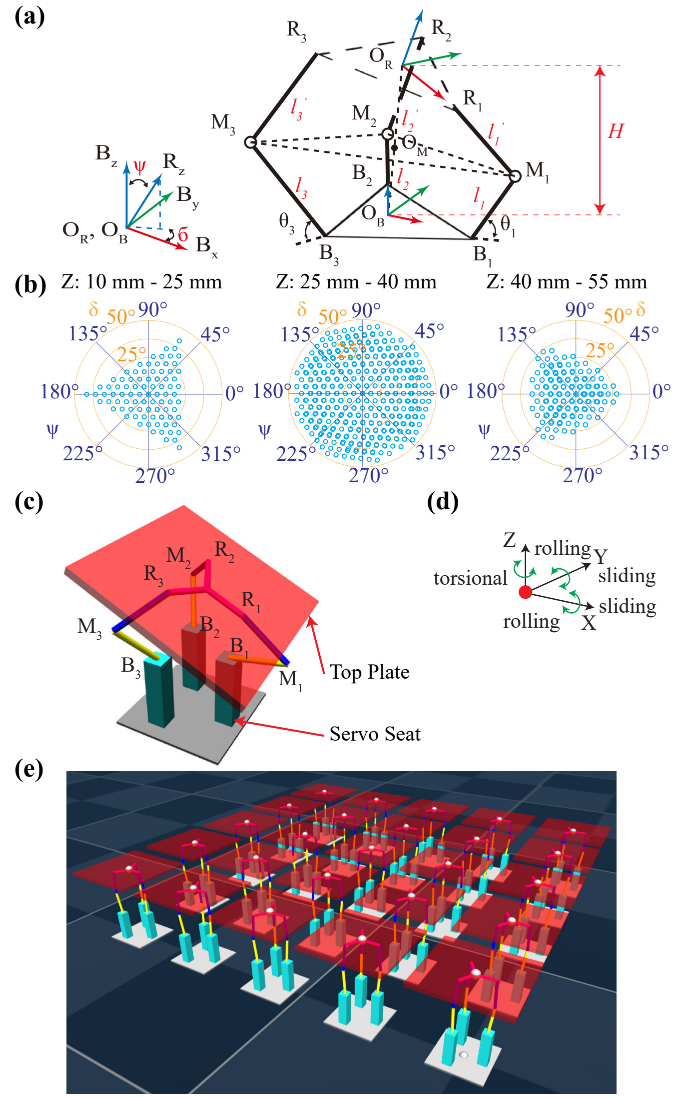

Fig. 2: **Kinematic model, workspace, and simulation setups.** (a) Kinematic model of the Canfield origami structure; (b) non-monotonic behavior of end-effector's workspace from lower to higher Z-height configurations, first expanding then contracting; (c) single module model for simulation; (d) simulation contact model; (e) 5×5 multi-module model for simulation.

II. Kinematic Modeling and Dynamic Simulation

This section discusses the kinematic modeling and workspace analysis of the Ori-Pixel platform, emphasizing its application in generating manipulation motion patterns. A dynamic model is then developed to simulate the dynamic behavior of the origami robot surface using MuJoCo [38].

A. Kinematic model and workspace analysis

This work uses a 5×5 grid of 25 3-DoF Canfield origami robots. Based on prior kinematic analyses [39], [40], the structure (Fig. 2(a)) consists of revolute joints $(B_1, B_2, B_3, R_1, R_2, R_3)$ and ball joints (M_1, M_2, M_3). All linkages $(l_1, l_2, l_3, l_1^{'}, l_2^{'}, l_3^{'})$ are 30 mm long, with $B_{1,2,3}$ and $R_{1,2,3}$ equidistant (20.21 mm) from centers O_B and O_R respectively. Actuation angles $\theta_i, i \in 1,2,3$ are determined from the top plate's pose parameters (δ, ψ, H) through:

$$\theta_i = 2 \cdot arctan(t_i), \theta_i \in [0, \frac{\pi}{2}], \tag{1}$$

where:

$$\begin{aligned} t_i &= \frac{-b_i \pm \sqrt{b_i^2 - 4a_i c_i}}{2a_i}, \\ a_i &= (r-l)(sin(\frac{\psi}{2}) \cdot cos(\delta - \theta_i)) - \frac{r_0}{2}, \\ b_i &= 2l \cdot cos(\frac{\psi}{2}), \\ c_i &= (r+l)(sin(\frac{\psi}{2}) \cdot cos(\delta - \theta_i)) - \frac{r_0}{2}, \\ r_0 &= \frac{H}{sin(\frac{\pi}{2} - \frac{\psi}{2})}. \end{aligned} \tag{2}$$

The end-effector's inclination angle (ψ) and height (H) are key parameters constrained by the system's kinematics. As depicted in Fig. 2(b), analysis of their workspace across three height configurations ($h \in [10, 25]$, $[25, 40]$ and $[40, 55]$ mm) reveals that the workspace first expands from lower to medium heights, then contracts at higher configurations. The workspace shows asymmetry across ψ and δ ranges, necessitating separate optimizations for each direction of manipulations.

B. Dynamic Simulation

The single-module model derived from the kinematic analysis is then developed for dynamic simulations in MuJoCo with a timestep of 5×10^{-4} s using the default semi-implicit Euler integrator. As illustrated in Fig. 2(c), the revolute joints B_1, B_2, B_3 are connected to the base of each lower linkage, with their axes offset by 60 degrees from one another. The ball joints M_1, M_2, M_3 link the lower linkages to the upper linkages, while the revolute joints R_1, R_2, R_3 connect the upper linkages to the top plate, sharing the same axis orientation as the joints B_1, B_2, B_3. A spring-damper model is applied to each joint, with a spring stiffness of $k_p = 0.2$ $N \cdot \text{m/rad}$ and a damping coefficient of $d = 0.1$ $N \cdot \text{m} \cdot \text{s/rad}$. The dimensions and masses of the linkages and top plates are derived from the same design parameters used in the prototype, as presented in [36]. Three motor actuators are implemented in position control mode with position feedback gain $k_p = 5$ and connected to the joints B_1, B_2, B_3.

The single-module model is then replicated to form the 5×5 module grid surface with identical distributions and dimensions as the prototype design presented in [36]. The multi-module MuJoCo model is depicted in Fig. 2(e). This model includes 75 motor actuators, and all top plates feature contact models to simulate interactions with objects using soft contact dynamics with a solver tolerance of 10^{-6} and a maximum 30 iterations per timestep. As illustrated in Fig. 2(d), the contact model incorporates sliding and rolling friction along the X and Y axes, and torsional friction along the Z axis. The sliding friction coefficient, μ_{slide}, and the rolling friction coefficient, μ_{roll}, are calibrated to 0.5 and 0.01, respectively.

III. CPG Motion Planning and Optimization for Manipulations

This section presents a novel CPG-based motion generation framework with simulation-based optimizations that, while demonstrated on Ori-Pixel platform, offer broad applicability across robotic systems. The proposed framework represents the first implementation of surface manipulations capable of handling diverse object geometries and stiffness. The following details the CPG parameter design, and the optimization framework across different manipulation modes.

A. CPG-based Manipulation Motion Planning

The CPG-based manipulation motion of a single 3-DoF Canfield origami robot mimics walking gait generation, consisting of three steps: object engagement through top plate lifting, object pushing through plate tilting, and plate retraction for disengagement, as shown in Fig. 3(a).

Sinusoidal functions are widely used in defining CPGs due to their smooth, periodic nature, which makes them ideal for generating stable and natural locomotion [41], [42]. Their simplicity enables efficient computation and easy phase adjustments, allowing synchronized movements that support coordinated, adaptive, and efficient control.

In this work, a sinusoidal-based CPG controller is developed to generate synchronized manipulation movements on the top plate of the robotic modules. These movements are described by coupled sinusoidal functions governing the height of the module's top plate, H, and the inclination angle of the top plate, ψ, as illustrated in Fig. 3(a). These two functions are coupled together to synchronously control the manipulation movements of the single module. The time-dependent variations of H and ψ are expressed as:

$$H(t) = h_{\text{amp}} \sin(2\pi f \cdot t + \phi) + h_0, \tag{3}$$

$$\psi(t) = \psi_{\text{amp}} \sin(2\pi f \cdot t + \phi + \sigma) + \psi_0, \tag{4}$$

where h_{amp} denotes the amplitude of the height variation, f is the frequency of motion, σ represents the phase shift coupling between H and ψ, h_0 and ψ_0 indicate the height and the inclination angle, respectively, of the top plate at its natural resting position, as depicted in Fig. 3(a). Additionally, ϕ represents the inter-group phase shift used to coordinate multiple groups of modules for effective manipulations.

As shown in Fig. 3(a), Eqs. (3) and (4) together define the motion pattern. The phase shift σ determines the inclination angle ψ when the top plate engages with the object, which dictates the manipulation direction. Specifically, if the first

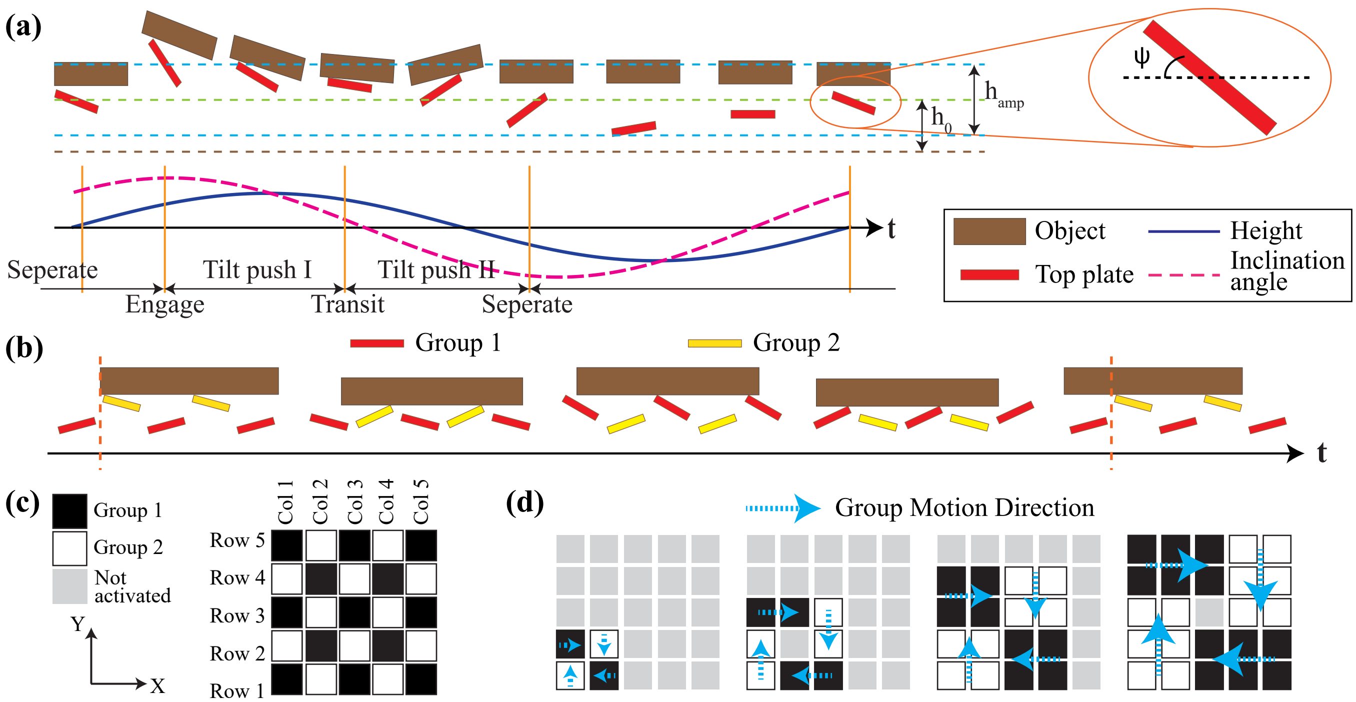

Fig. 3: **CPG motion plan and inter-group motion plan.** (a) Single module motion plan; (b) multi-module manipulation motion plan. (c) inter-group motion planning for translation manipulations; (d) motion planning for clock-wise rotation manipulation.

contact occurs during the tilt push I phase, where $\sigma \in [0, \pi)$, the manipulation direction is toward the left-hand side; if the first contact occurs during the tilt push II phase, where $\sigma \in [-\pi, 0)$, the direction shifts to the right-hand side. Furthermore, the phase shift σ influences both the floating and tilting ranges of the object during manipulation, playing a key role in balancing the trade-off between speed and smoothness in the overall performance. This trade-off will be further studied during the optimization process in Section III-B.

While single modules can complete manipulation cycles (Fig. 3(a)), additional module support during plate retraction is needed to prevent backward slippage. Thus, modules are divided into two groups using Eqs. (3) and (4) with identical parameters except for an inter-group phase shift ϕ. As depicted in Fig. 3(b), this coordination enables simultaneous pushing and supporting motions for effective manipulations.

B. Collective motion planning for manipulations using multi-module robotic surface

The inter-group motion plan developed for translational manipulations on the Ori-Pixel platform divides the modules into two diagonal groups, with their motion generated by the CPG described in Section III-A, as depicted in Fig. 3(c). These groups are synchronized through the inter-group phase shift term, ϕ. The diagonal symmetric configuration maintains object orientation during movement by applying forces without rotational torque, ensuring robust and stable motion.

The direction of translational manipulation is determined by two parameters: the azimuth angle δ (which defines the manipulation axis: $\delta = 0$ degree for Y-axis and $\delta = 90$ degree for X-axis as shown in Fig. 2(a) and Fig. 3(c)), and the inter-group phase shift σ (which determines direction along the chosen axis: $\sigma \in [0, \pi)$ for positive and $\sigma \in [-\pi, 0)$ for negative direction, as detailed in Section III-A). Together, these parameters enable omni-directional planar manipulation.

The rotational manipulation plan coordinates modules' translational movements in different directions. Objects must contact at least two by two top plates. Two module groups operate with $\phi = \pi$ phase shift. As shown in Fig. 3(d), Group 1 moves along X-axis (positive in top-left, negative in bottom-right), while Group 2 moves along Y-axis (negative in top-right, positive in bottom-left) for clockwise rotation. Counter-clockwise rotation reverses these directions while maintaining ϕ, ensuring continuous rotational manipulation.

In addition to the motion plans, the top plate's effective contact ratio ($S_{contact}/S_{plate}$) is crucial for manipulations, where $S_{contact}$ represents the object-covered area and S_{plate} the total plate area. Modules are activated when this ratio exceeds a threshold ϵ, otherwise returning to rest. This threshold, analyzed during optimization, ensures effective manipulation without obstruction. The complete control framework is illustrated in Fig. 4(a).

C. Optimization Framework for Manipulation Motions

A simulation-based optimization framework is developed to identify the optimal CPG parameters for different manipulation modes and objects, using the motion planned in Section III-B. The complete process is elaborated in Fig. 4(b).

The proposed framework utilizes the simulation model from Section II-B, integrated with an evolutionary Bayesian hyperparameter optimizer [43] to identify optimal parameter sets for different manipulation modes. The optimization search

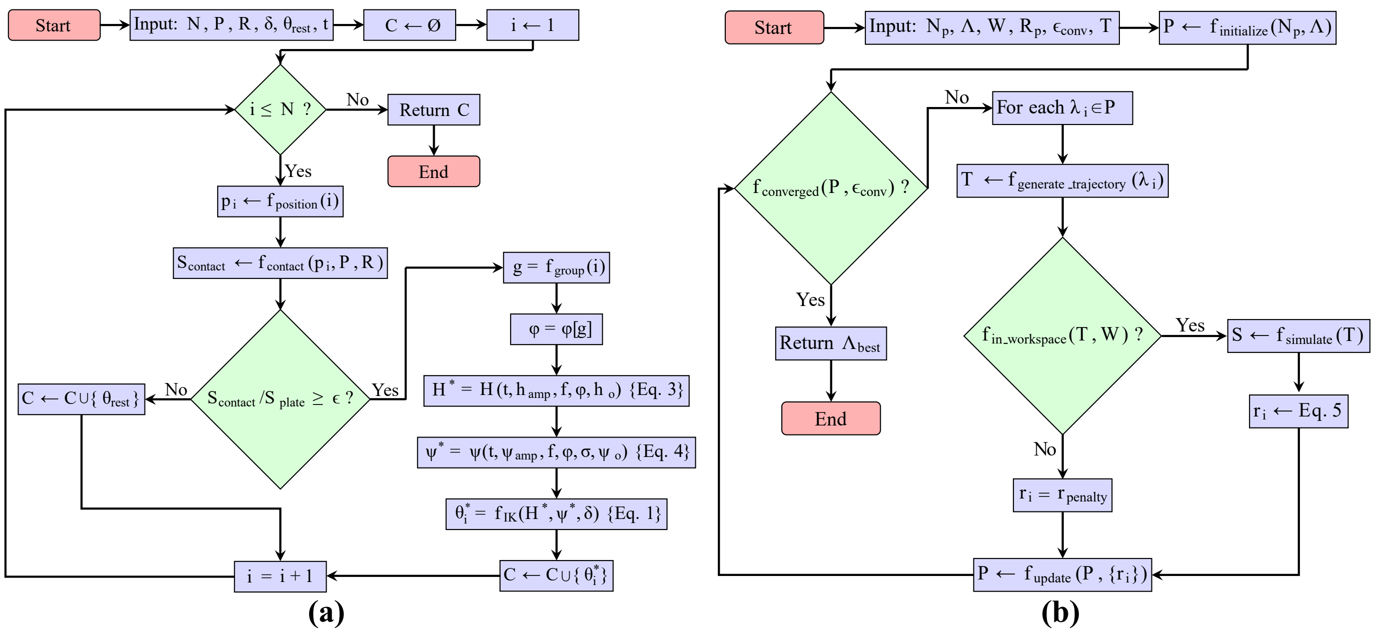

Fig. 4: **Control and Optimization Frameworks.** (a) Control framework for CPG-based manipulation; (b) optimization framework for CPG parameters.

space spans eight parameters $h_{\text{amp}}, \psi_{\text{amp}}, f, h_0, \psi_0, \phi, \delta, \epsilon$ from Equations (3) and (4). The amplitude and frequency ranges in Table I were bounded by our servo motors' physical limits. The initial height h_0 and orientation ψ_0 ranges were determined by the prototype's geometric design and kinematic workspace analysis as in Section II-A, while the phase parameters were constrained to ensure smooth transitions between motion states. During the optimization process, the object is positioned at the center of one side of the robotic surface. The modules are commanded to move for 5 seconds following the control protocol outlined in Fig. 4(a), using the parameters suggested by the optimizer. The object's travel distance, Z-axis displacement, and rotation angles during the movement are evaluated using a cost function, which serves as reward feedback for the optimizer.

TABLE I: Optimization Search Space

Parameter	Symbol	Search Space	Unit
Height amplitude	h_{amp}	[0.005, 0.04]	m
Inclination angle amplitude	ψ_{amp}	$[0.35, 0.79]$	radian
Frequency	f	$[0.1, 0.8]$	Hz
Resting height	h_0	$[0.02, 0.04]$	m
Resting inclination angle	ψ_0	$[-0.26, 0.26]$	radian
Height-inclination phase shift	σ	$[0, \pi]$ or $[\pi, 2\pi]$	radian
Inter-group phase shift	ϕ	$[0, 2\pi]$	radian
Top plate contact threshold	ϵ	$[0.1, 0.5]$	-

A generalized cost function J is constructed to assess manipulation performance, incorporating various manipulation objectives. As shown in Eq. (5), the cost function accounts for the object's absolute averaged translational speed v, the absolute averaged yaw speed ω, the max roll (η) and pitch (ρ) angles, as well as the max displacement in z-direction throughout the manipulation process. The weights $\{\alpha, \beta, \gamma, \varsigma\}$ can be tuned to prioritize different manipulation objectives.

$$J = \alpha \cdot v + \beta \cdot \omega + \gamma \cdot \left(\max_t \eta(t) + \max_t \rho(t) \right) + \varsigma \cdot \max_t z(t). \tag{5}$$

For fast manipulations, where only the object's average manipulation speed v is considered, the weights are set to $\{\alpha, \beta, \gamma, \varsigma\} = \{-1, 0, 0, 0\}$, ensuring that the optimizer focuses on maximizing the manipulation speed. In contrast, for smooth manipulations aimed at minimizing rotation, tilting, and shaking, the weights are adjusted to $\{\alpha, \beta, \gamma, \varsigma\} = \{-0.2, 0.3, 0.3, 0.3\}$, which directs the optimizer to prioritize reducing pose variations during the manipulation while still maintaining a reasonable speed. For rotational manipulations, the weights are set to $\{\alpha, \beta, \gamma, \varsigma\} = \{1, -1, 0, 0\}$, penalizing translational motions while rewarding yaw rotations.

Using the optimization framework and simulation environments from Section II-B, we optimized CPG parameters (Table I) for various manipulation motions (omnidirectional planar translations in fast/smooth modes and pure rotations). Due to the asymmetric workspace as discussed in Section II-A, each case was optimized separately. For fast modes, we fixed $\phi = \pi$ to maximize contact time, while for smooth modes, ϕ was optimized to control contact transitions and minimize vertical displacement. The framework converged in 30 minutes on an AMD Ryzen Threadripper 7960X with 128GB RAM. Results are shown in supplementary video 1.

IV. CPG-BASED MANIPULATIONS ON PROTOTYPE

This section describes the laboratory experiments conducted with the Ori-Pixel robotic surface to manipulate various objects using the optimized CPG motions from Section III.

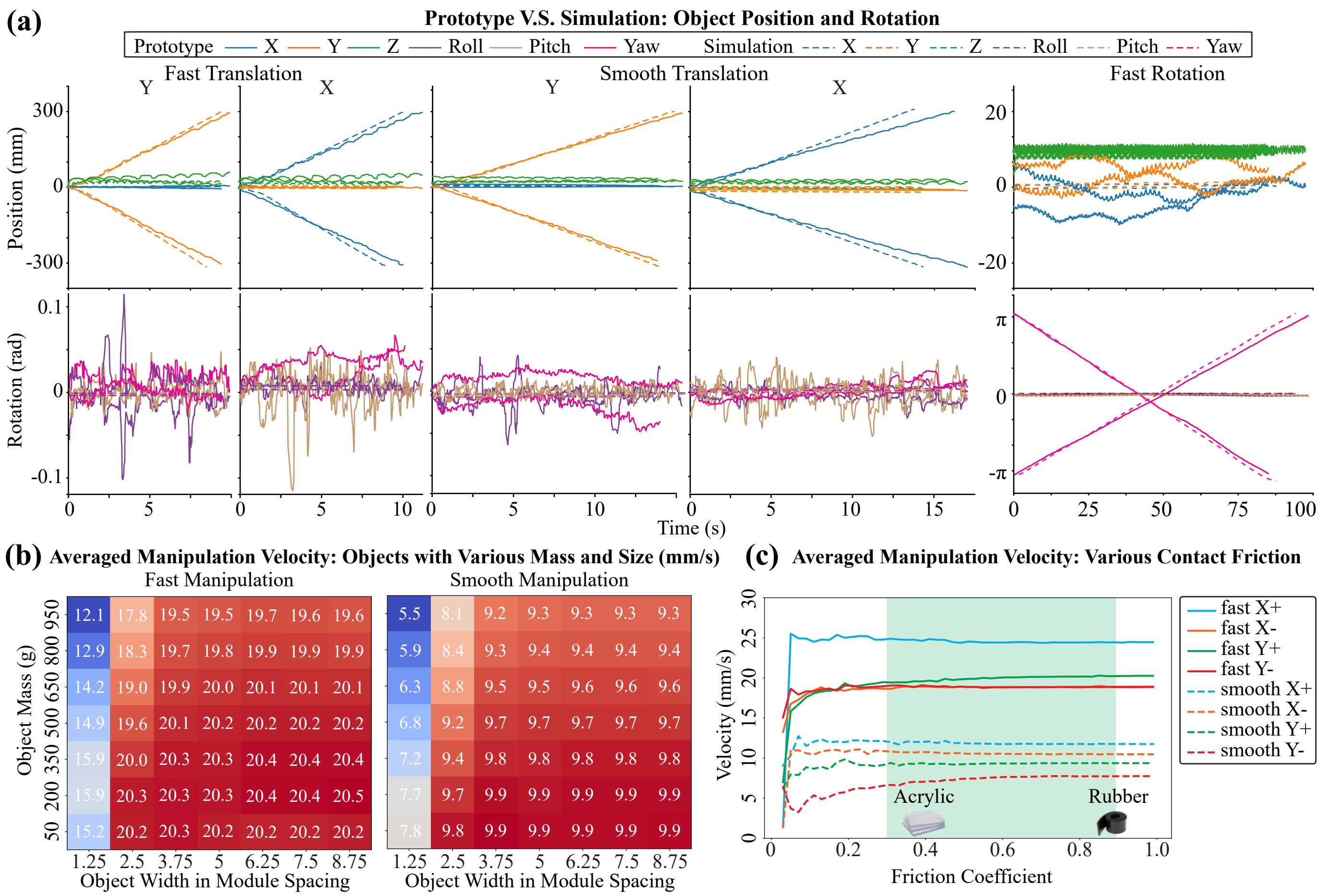

Fig. 5: **Prototype and Simulation Results.** (a) Simulated and prototype results for translational and rotational manipulations. (b) Averaged manipulation velocity from simulation for various object masses and widths using the Ori-pixel module spacing of 120 mm as a reference unit; (c) averaged manipulation velocity from simulation with various contact friction coefficients.

A. *Experiment Setup*

The Ori-Pixel robotic surface, comprising 25 modules each actuated by three Dynamixel XL-320 servos operating at 20 Hz in position mode, is used for laboratory experiments (Fig. 1(a)). A Vicon Vero motion tracking system provides real-time object pose data for module activation control following Fig. 4(a). Experiments are conducted with objects of varying size, weight, shape, and stiffness, as listed in Table II.

TABLE II: Properties of Tested Objects

Index	Shape	Material	Size (mm)	Mass (g)	Tested Modes
i	Plate	Acrylic	300×300	254	Fast, Smooth
ii	Plate	Wood	200×200	172	Fast, Smooth
iii	Cylinder	Foam	⌀36×140	9	Smooth
iv	Plate	Acrylic	1000×300	1000	Fast
v	Polo shirt	Fabric	400×400	280	Fast
vi	Trilby hat	Straw	270×250	55	Fast

B. *CPG-Based Manipulation Experiments on Ori-pixel*

The optimized CPG parameters are applied to manipulate a spectrum of objects as listed in Table II. The system successfully manipulated objects ranging from a small plate (ii) to a much larger plate (iv), demonstrating the optimized motion's ability to handle a wide size range. The system also successfully manipulated objects with flexible materials and irregular shapes (v, vi) where position tracking becomes challenging. The platform operates in open-loop mode, with all modules activated following optimized CPG motions without position feedback. These experiments demonstrate that motions derived using the proposed framework can successfully handle objects of varying sizes, shapes, and stiffness, showcasing the robustness and versatility of the proposed manipulation strategy. Complete documentation is available in supplementary video 2.

We evaluated the fast and smooth manipulation modes using object i as depicted in Fig. 5(a). Fast manipulation achieved higher velocities (30 mm/s Y-direction, 25 mm/s X-direction) compared to smooth manipulation (20 mm/s Y-direction, 17 mm/s X-direction). However, smooth manipulation demonstrated superior stability with lower Z-direction displacement (averaged standard deviation: 3.03 mm vs 7.05 mm) and rotation angles (averaged standard deviation: 0.0091 rad vs 0.0133 rad). To demonstrate stability, we successfully manipulated object i while supporting an unrestrained object iii (Figure 1(b)(iii)). Pure rotational tests achieved average angular velocities of 0.079 rad/s clockwise and 0.063 rad/s counterclockwise. All experiments are documented in supplementary video 3.

C. Sim-to-real Analysis

To analyze the sim-to-real discrepancy, we conducted simulations using object i with optimized CPG-based control parameters and compared them with experimental results, as shown in Fig. 5(a). The simulation demonstrates strong alignment with the actual dynamic behavior during manipulation, though some differences were observed—specifically in rotation data during translation modes and position data during rotation modes. These discrepancies are primarily attributed to actuation delays between servos in the physical platform and natural variations in object placement during trials.

Despite these differences, the control parameters optimized in simulation transferred effectively to real-world implementation, validating the robustness of our approach. The observed sim-to-real deviation is within acceptable bounds, as the CPG gaits from simulation consistently yield effective results in prototyping tests, further supporting the strong correlation between simulation and real-world performance.

D. Conclusion

This section evaluated the CPG-based manipulation motions derived from the simulation-based optimization process through prototype experiments. The experiments demonstrated high-fidelity sim-to-real transfer and validated the proposed framework by successfully manipulating objects of various size, shape, and stiffness, while executing fast and smooth manipulation modes to meet different performance requirements.

V. Discussion

This section analyzes experimental results to evaluate our CPG-based manipulation framework. We demonstrate the framework's robustness across varying object properties (mass and size) and contact friction conditions, followed by a discussion of its key assumptions and limitations.

A. Robustness Analysis

For robustness analysis of our proposed CPG-based manipulation framework, we conducted a series of simulations with the Ori-pixel platform serving as our experimental testbed. We analyzed box-shaped objects with a fixed height of 50 mm but varying mass and width. The mass ranged from 50 g to 950 g in 150 g increments, and using the Ori-pixel module spacing of 120 mm as a reference unit, we varied object widths from 1.25 to 8.75 module spans in 1.25-span increments. We simulated translational manipulations in all directions using fast and smooth modes, with results shown in Fig. 5(b). The analysis reveals that manipulation performance strongly correlates with module coverage, where objects spanning 2×2 modules result in manipulation that is more sensitive to object properties and achieves lower velocities, while coverage of 3×3 modules or more enables robust, high-velocity manipulation. This improved performance with larger coverage stems from better load distribution across modules, which helps mitigate the velocity reduction effects from increasing object mass. These results demonstrate the framework's robustness across a range of object masses and sizes.

We then investigated the effect of contact friction between the object and the platform. Using the same simulation setup with object i as in Table II, we varied the friction coefficient from 0.02 to 1 in 0.02 increments, testing all directional translational manipulations in both fast and smooth modes. The average velocities are shown in Fig. 5(c). At friction coefficients below 0.3, manipulation velocity shows unstable saturation behavior. Above 0.3, the velocity stabilizes, indicating robust performance. The green shaded region (0.3-0.9) highlights that our proposed manipulation method works effectively with common materials ranging from acrylic (friction coefficient 0.4) to rubber (friction coefficient 0.9).

B. Assumptions and Limitations

The manipulation method presented here demonstrates robust performance across objects with diverse shapes, sizes, weights, and materials. For implementation on the current Ori-pixel platform, we assume objects have a flat contact surface, are larger than 150 mm to effectively cover more than 2×2 tiles and prevent falling into gaps between modules, and weigh less than 1500 g due to actuator capabilities.

As for the limitations of the proposed framework, the robust manipulation performance requires friction coefficients above 0.3, though this encompasses most common materials from acrylic to rubber. Additionally, the framework has a resolution limitation requiring objects to span at least 2×2 tiles to maintain consistent manipulation forces.

VI. Conclusion and Future Work

This letter introduces a novel manipulation framework that uses a CPG-based motion generator to enable manipulation motions on a multi-module origami robotic surface. It also presents a simulation-based optimization method to find the best CPG parameters for various manipulation goals. The optimized manipulation motions are evaluated using both dynamic simulations and prototype experiments. This letter also showcases a series of demonstration experiments using the optimal CPG motions to manipulate objects of different sizes, shapes, and stiffness, highlighting robust and versatile manipulation across a wide range of objects.

In future work, reconfigurable module layouts will be investigated to enhance the platform's versatility. This improvement aims to expand the range of objects that can be effectively manipulated. Additionally, we plan to explore hybrid frameworks that combine learning-based methods with CPG to balance adaptability and control efficiency. Furthermore, we plan to explore hybrid frameworks that combine learning-based methods with CPG to enable more dynamic and complex manipulation tasks while maintaining control efficiency.

REFERENCES

[1] J. Shintake and other, "Versatile Soft Grippers with Intrinsic Electroadhesion Based on Multifunctional Polymer Actuators," *Advanced Materials*, vol. 28, no. 2, pp. 231–238, Jan. 2016.

[2] J. Shintake, V. Cacucciolo, D. Floreano, and H. Shea, "Soft Robotic Grippers," *Advanced Materials*, vol. 30, no. 29, p. 1707035, Jul. 2018.

[3] H. Khurana and A. Billard, "Motion Planning and Inertia-Based Control for Impact Aware Manipulation," *IEEE Transactions on Robotics*, vol. 40, pp. 2201–2216, 2024.

[4] J. Cui and J. Trinkle, "Toward next-generation learned robot manipulation," *Science Robotics*, vol. 6, no. 54, p. eabd9461, May 2021.

[5] S. Abondance, C. B. Teeple, and R. J. Wood, "A Dexterous Soft Robotic Hand for Delicate In-Hand Manipulation," *IEEE Robotics and Automation Letters*, vol. 5, no. 4, pp. 5502–5509, Oct. 2020.

[6] O. M. Andrychowicz, B. Baker, M. Chociej, R. Józefowicz, B. McGrew, J. Pachocki, A. Petron, M. Plappert, G. Powell, A. Ray, J. Schneider, S. Sidor, J. Tobin, P. Welinder, L. Weng, and W. Zaremba, "Learning dexterous in-hand manipulation," *The International Journal of Robotics Research*, vol. 39, no. 1, pp. 3–20, Jan. 2020.

[7] H. Liu, L. Zhao, B. Siciliano, and F. Ficuciello, "Modeling, Optimization, and Experimentation of the ParaGripper for In-Hand Manipulation Without Parasitic Rotation," *IEEE Robotics and Automation Letters*, vol. 5, no. 2, pp. 3011–3018, Apr. 2020.

[8] J. Aldaco *et al.*, "Aloha 2: An enhanced low-cost hardware for bimanual teleoperation," 2024. [Online]. Available: https://arxiv.org/abs/2405.02292

[9] K. Darvish, L. Penco, J. Ramos, R. Cisneros, J. Pratt, E. Yoshida, S. Ivaldi, and D. Pucci, "Teleoperation of humanoid robots: A survey," *IEEE Transactions on Robotics*, vol. 39, no. 3, pp. 1706–1727, 2023.

[10] M. Sharifzadeh, Y. Jiang, A. S. Lafmejani, and D. M. Aukes, "Compensating for material deformation in foldable robots via deep learning — a case study," in *2022 International Conference on Robotics and Automation (ICRA)*, 2022, pp. 5184–5190.

[11] Y. Liu and A. Billard, "Tube Acceleration: Robust Dexterous Throwing Against Release Uncertainty," *IEEE Transactions on Robotics*, vol. 40, pp. 2831–2849, 2024.

[12] F. Zhang and Y. Demiris, "Learning garment manipulation policies toward robot-assisted dressing," *Science Robotics*, vol. 7, no. 65, p. eabm6010, Apr. 2022.

[13] J. Shintake, V. Cacucciolo, D. Floreano, and H. Shea, "Soft robotic grippers," *Advanced materials*, vol. 30, no. 29, p. 1707035, 2018.

[14] W. Crooks, S. Rozen-Levy, B. Trimmer, C. Rogers, and W. Messner, "Passive gripper inspired by manduca sexta and the fin ray® effect," *International Journal of Advanced Robotic Systems*, vol. 14, no. 4, p. 1729881417721155, 2017.

[15] N. G. Cheng, M. B. Lobovsky, S. J. Keating, A. M. Setapen, K. I. Gero, A. E. Hosoi, and K. D. Iagnemma, "Design and analysis of a robust, low-cost, highly articulated manipulator enabled by jamming of granular media," in *2012 IEEE International Conference on Robotics and Automation*, 2012, pp. 4328–4333.

[16] S. Sun, H. Deng, H. Du, W. Li, J. Yang, G. Liu, G. Alici, and T. Yan, "A compact variable stiffness and damping shock absorber for vehicle suspension," *IEEE/ASME Transactions on Mechatronics*, vol. 20, no. 5, pp. 2621–2629, 2015.

[17] J. Shintake, S. Rosset, B. Schubert, D. Floreano, and H. Shea, "Versatile soft grippers with intrinsic electroadhesion based on multifunctional polymer actuators," *Advanced Materials*, vol. 28, no. 2, pp. 231–238, 2016.

[18] E. W. Hawkes, D. L. Christensen, A. K. Han, H. Jiang, and M. R. Cutkosky, "Grasping without squeezing: Shear adhesion gripper with fibrillar thin film," in *2015 IEEE International Conference on Robotics and Automation (ICRA)*. IEEE, 2015, pp. 2305–2312.

[19] D. Leithinger, S. Follmer, A. Olwal, and H. Ishii, "Shape Displays: Spatial Interaction with Dynamic Physical Form," *IEEE Computer Graphics and Applications*, vol. 35, no. 5, pp. 5–11, Sep. 2015.

[20] D. R. Barr, D. Walsh, and P. Dudek, "A smart surface simulation environment," in *2013 IEEE International Conference on Systems, Man, and Cybernetics*. IEEE, 2013, pp. 4456–4461.

[21] S. Follmer, D. Leithinger, A. Olwal, A. Hogge, and H. Ishii, "inFORM: dynamic physical affordances and constraints through shape and object actuation," in *Proceedings of the 26th annual ACM symposium on User interface software and technology*. ACM, 2013, pp. 417–426.

[22] Z. Xue *et al.*, "Arraybot: Reinforcement learning for generalizable distributed manipulation through touch," 2025. [Online]. Available: https://arxiv.org/abs/2306.16857

[23] S. Thompson, P. Mannam, Z. Temel, and O. Kroemer, "Towards Robust Planar Translations using Delta-manipulator Arrays," in *2021 IEEE International Conference on Robotics and Automation (ICRA)*. Xi'an, China: IEEE, May 2021, pp. 6563–6569.

[24] S. Patil, T. Tao, T. Hellebrekers, O. Kroemer, and F. Z. Temel, "Linear delta arrays for compliant dexterous distributed manipulation," in *2023 IEEE International Conference on Robotics and Automation (ICRA)*. IEEE, 2023, pp. 10 324–10 330.

[25] Z. Deng, M. Stommel, and W. Xu, "A Novel Soft Machine Table for Manipulation of Delicate Objects Inspired by Caterpillar Locomotion," *IEEE/ASME Transactions on Mechatronics*, vol. 21, no. 3, pp. 1702–1710, Jun. 2016.

[26] M. A. Robertson, M. Murakami, W. Felt, and J. Paik, "A Compact Modular Soft Surface With Reconfigurable Shape and Stiffness," *IEEE/ASME Transactions on Mechatronics*, vol. 24, no. 1, pp. 16–24, Feb. 2019.

[27] M. Ataka, B. Legrand, L. Buchaillot, D. Collard, and H. Fujita, "Design, Fabrication, and Operation of Two-Dimensional Conveyance System With Ciliary Actuator Arrays," *IEEE/ASME Transactions on Mechatronics*, vol. 14, no. 1, pp. 119–125, Feb. 2009.

[28] K. Liu, F. Hacker, and C. Daraio, "Robotic surfaces with reversible, spatiotemporal control for shape morphing and object manipulation," *Science Robotics*, vol. 6, no. 53, p. eabf5116, Apr. 2021.

[29] A. Badri-Spröwitz, A. Aghamaleki Sarvestani, M. Sitti, and M. A. Daley, "BirdBot achieves energy-efficient gait with minimal control using avian-inspired leg clutching," *Science Robotics*, vol. 7, no. 64, p. eabg4055, 2022.

[30] G. Li, A. Ijspeert, and M. Hayashibe, "Ai-cpg: Adaptive imitated central pattern generators for bipedal locomotion learned through reinforced reflex neural networks," *IEEE Robotics and Automation Letters*, vol. 9, no. 6, pp. 5190–5197, 2024.

[31] Y. Fukuoka, H. Kimura, and A. H. Cohen, "Adaptive dynamic walking of a quadruped robot on irregular terrain based on biological concepts," *The International Journal of Robotics Research*, vol. 22, no. 3-4, pp. 187–202, 2003.

[32] A. Spröwitz, A. Tuleu, M. Vespignani, M. Ajallooeian, E. Badri, and A. J. Ijspeert, "Towards dynamic trot gait locomotion: Design, control, and experiments with cheetah-cub, a compliant quadruped robot," *The International Journal of Robotics Research*, vol. 32, no. 8, pp. 932–950, 2013.

[33] X. Liu, C. D. Onal, and J. Fu, "Reinforcement learning of cpg-regulated locomotion controller for a soft snake robot," *IEEE Transactions on Robotics*, vol. 39, no. 5, pp. 3382–3401, 2023.

[34] M. Porez, F. Boyer, and A. J. Ijspeert, "Improved lighthill fish swimming model for bio-inspired robots: Modeling, computational aspects and experimental comparisons," *The International Journal of Robotics Research*, vol. 33, no. 10, pp. 1322–1341, 2014.

[35] A. Crespi and A. J. Ijspeert, "Online optimization of swimming and crawling in an amphibious snake robot," *IEEE Transactions on Robotics*, vol. 24, no. 1, pp. 75–87, 2008.

[36] M. Salerno, J. Paik, and S. Mintchev, "Ori-pixel, a multi-dofs origami pixel for modular reconfigurable surfaces," *IEEE Robotics and Automation Letters*, vol. 5, no. 4, pp. 6988–6995, 2020.

[37] Z. Wang, S. Demirtas, F. Zuliani, and J. Paik, "Surface-based manipulation," 2025. [Online]. Available: https://arxiv.org/abs/2502.19389

[38] E. Todorov, T. Erez, and Y. Tassa, "Mujoco: A physics engine for model-based control," in *2012 IEEE/RSJ International Conference on Intelligent Robots and Systems*. IEEE, 2012, pp. 5026–5033.

[39] S. L. Canfield and C. F. Reinholtz, "Development of the carpal robotic wrist," in *Experimental Robotics V*, A. Casals and A. T. de Almeida, Eds. Berlin, Heidelberg: Springer Berlin Heidelberg, 1998, pp. 423–434.

[40] M. Mete, J.-L. Huang, and J. Paik, "Dynamic modeling of an origami prismatic joint," in *2023 IEEE International Conference on Soft Robotics (RoboSoft)*, 2023, pp. 1–6.

[41] A. J. Ijspeert, "Central pattern generators for locomotion control in animals and robots: A review," *Neural Networks*, vol. 21, no. 4, pp. 642–653, May 2008, publisher: Elsevier BV.

[42] L. Righetti and A. J. Ijspeert, "Pattern generators with sensory feedback for the control of quadruped locomotion," in *2008 IEEE International Conference on Robotics and Automation*, 2008, pp. 819–824.

[43] A. I. Cowen-Rivers *et al.*, "Hebo: Pushing the limits of sample-efficient hyperparameter optimisation," *Journal of Artificial Intelligence Research*, vol. 74, 07 2022.